Afsaneh Labbaf, Maurice Dellin, Marlene Komadowski, Dane M. Chetkovich, Niels Decher, Hans-Chrisitian Pape, Guiscard Seebohm, Thomas Budde* and Mehrnoush Zobeiri*

Characterization of Kv1.2-mediated outward current in TRIP8b-deficient mice

https://doi.org/10.1515/hsz-2023-0116
Received January 30, 2023; accepted February 16, 2023;
published online March 1, 2023

Abstract: Tonic current through hyperpolarization-activated cyclic nucleotide-gated cation (HCN) channels is influencing neuronal firing properties and channel function is strongly influenced by the brain-specific auxiliary subunit tetratricopeptide repeat-containing Rab8b-interacting protein (TRIP8b). Since Kv1.2 channels and TRIP8b were also suggested to interact, we assessed brain Kv1.2 mRNA and protein expression as well as the reduction of K^+ outward currents by Kv1.2-blocking compounds (Psora-4; tityustoxin-Kα, TsTX-Kα) in different brain areas of *TRIP8b*-deficient (*TRIP8b*$^{-/-}$) compared to wildtype (WT) mice. We found that transcription levels of Kv1.2 channels were not different between genotypes. Furthermore, Kv1.2 current amplitude was not affected upon co-expression with TRIP8b in oocytes. However, Kv1.2 immunofluorescence was stronger in dendritic areas of cortical and hippocampal neurons. Furthermore, the peak net outward current was increased and the inactivation of the Psora-4-sensitive current component was less pronounced in cortical neurons in *TRIP8b*$^{-/-}$ mice. In current clamp recordings, application of TsTX increased the excitability of thalamocortical (TC) neurons with increased number of elicited action potentials upon step depolarization. We conclude that TRIP8b may not preferentially influence the amplitude of current through Kv1.2 channels but seems to affect current inactivation and channel localization. In *TRIP8b*$^{-/-}$ a compensatory upregulation of other Kv channels was observed.

Keywords: action potential firing; K^+ current; Kv channel blocker; oocytes; thalamus; TRIP8b.

Introduction

The diversity of ion channel functions is based on the existence of several α subunit gene families but also on a multitude of regulatory β subunits that co-assemble with the α subunits to modulate aspects of their function (Abbott 2012). Surprisingly, some of the β subunits are promiscuous and interact with members of more or less related ion channel families. In this respect, KCNE2 is a prototypical example since it forms complexes with several different Kv channels and has the capacity to regulate HCN channels (Decher et al. 2003). The brain-specific auxiliary subunit of HCN channels TRIP8b may exert similar diversified regulatory influences (Han et al. 2020). Indeed, apart from HCN channels, the Kv1.2 mediated current has been reported to show an increase of about 15% when the channels were co-expressed with the TRIP8b 1a-4 isoform in oocytes (Santoro et al. 2009). Importantly, HCN channels, KCNE2, Kv1.2 channels and TRIP8b have all been shown to be relevant for TC activity and altered function is associated with epilepsy (Alkire et al. 2009; Cazzin et al. 2011; Kanyshkova et al. 2012; Ying et al. 2012; Zobeiri et al. 2018). TRIP8b is a cytosolic protein consisting of several splice variants, each differentially controlling HCN channel trafficking and gating in a subtype-specific manner (Lewis et al. 2009; Santoro et al. 2004, 2009, 2011). Mice with global elimination of TRIP8b protein (*TRIP8b*$^{-/-}$ mice) show lower expression levels for HCN channels in both cortex (mostly expressing HCN1 and HCN2 subunits) and thalamus (mostly expressing HCN2 and HCN4 subunits) and exhibit sporadic spike-and-wave discharges (SWDs) characteristic of absence epilepsy (Heuermann et al. 2016; Zobeiri et al. 2018). Reduced expression of HCN1 channels in cortical pyramidal neurons of *TRIP8b*$^{-/-}$ mice is associated with hyperpolarizing effects on resting membrane potential (RMP) and increased input resistance (R_{input}) and consequently increased excitability of these

***Corresponding authors: Thomas Budde and Mehrnoush Zobeiri**, Institut für Physiologie I, Wilhelms-Universität, Robert-Koch-Str. 27a, D-48149 Münster, Germany, E-mail: tbudde@uni-muenster.de (T. Budde), zobeiri@uni-muenster.de (M. Zobeiri).
https://orcid.org/0000-0002-5263-8183 (T. Budde)
Afsaneh Labbaf and Hans-Chrisitian Pape, Institute of Physiology I, Westfälische Wilhelms-Universität, Robert-Koch-Str. 27a, D-48149 Münster, Germany
Maurice Dellin and Guiscard Seebohm, Department of Cardiovascular Medicine, Institute for Genetics of Heart Diseases (IfGH), University Hospital Münster, Robert-Koch-Str. 45, D-48149 Münster, Germany
Marlene Komadowski and Niels Decher, Institute of Physiology and Pathophysiology, Vegetative Physiology, Philipps-University of Marburg, Deutschhausstr. 1-2, 35037, Marburg, Germany
Dane M. Chetkovich, Medical Center, Department of Neurology, Vanderbilt University, Nashville, TN, USA

neurons (Heuermann et al. 2016; Lewis et al. 2011). Similarly, mice lacking the HCN1 subunit (*HCN1*$^{-/-}$ mice) show enhanced pyramidal cell excitability (Huang et al. 2009) and higher susceptibility to generate seizures (Huang et al. 2009). In TC neurons, loss of TRIP8b results in reduced cell surface expression of both HCN2 and HCN4 and therefore decreased I_h density and is associated with decreased tonic firing and increased propensity for burst firing in response to depolarizing inputs (Zobeiri et al. 2018). Although TRIP8b was shown to affect HCN channels expression and gating in the thalamus, the extent of the changes in the excitability of TC neurons in TRIP8b$^{-/-}$ mice could not be solely explained by TRIP8b interaction with HCN channels (Zobeiri et al. 2018). In *HCN2*$^{-/-}$ mice, TC neurons exhibit a significant reduction in tonic firing, as well as, a clear shift from tonic to burst firing upon injection of positive current steps from RMP (Ludwig et al. 2003). Surprisingly, loss of the major thalamic channel isoform in HCN4-deficient mice (HCN4$^{-/-}$), is associated with decreased I_h density, but in contrary to *HCN2*$^{-/-}$ and *TRIP8b*$^{-/-}$, increased tonic firing in TC neurons (Zobeiri et al. 2019). These findings therefore indicated the involvement of additional compensatory factors in regulating the excitability of TC neurons in *TRIP8b*$^{-/-}$ mice.

Apart from HCN channels, the current mediated by Kv1.2 is moderately influenced by TRIP8b in oocyte expression systems (Santoro et al. 2009). While increased activity of A-type K^+ channels in TC neurons in *TRIP8b*$^{-/-}$ mice has been found (Zobeiri et al. 2018), it is not clear whether changes in firing pattern are possibly influenced by concomitant downregulation of Kv1.2 channels due to TRIP8b loss. Kv1.2 channels belong to the family of low-voltage activated potassium channels that activate upon depolarization to voltages around the threshold for AP generation and produce a sustained outward current in neurons. Kv1.2 channels play important and diverse roles in regulating excitability of axons, nerve terminals, and dendrites of mammalian neurons (Dodson and Forsythe 2004). Presynaptic Kv1.2 channels are important in preventing hyperexcitability in both central and peripheral neurons. While the overexpression of Kv1.2 in central medial (CM) TC neurons in rats attenuates tonic discharges (Cazzin et al. 2011), the contribution of these channels to basal tonic activity is less clear. Therefore, we tried to assess whether Kv1.2 channels properties are changed in *TRIP8b*$^{-/-}$ mice and limit tonic firing in TC neurons. We studied Kv1.2 mRNA levels in mouse brain. In addition, we compared the reduction of K^+ outward currents by Kv1.2-blocking compounds (Psora-4; TsTX-Kα) in different brain areas (hippocampal regions CA1 and CA3; somatosensory cortex, SSC; ventrobasal thalamic complex, VB) of *TRIP8b*$^{-/-}$ and WT mice. In the same brain regions, we analyzed the protein expression of Kv1.2 channels by immunofluorescence staining. Furthermore, we co-expressed Kv1.2 channels and TRIP8b in oocytes. Although Kv1.2 channels effectively control tonic firing in TC neurons and the distribution of channel protein is more dispersed in some brain regions of *TRIP8b*$^{-/-}$ mice, it is unlikely that changes in Kv1.2 channel function contribute to altered firing pattern of TC neurons in these knockout animals. Nevertheless, the loss of TRIP8b seems to induce compensatory upregulation of other Kv channels.

Results

Since Kv1.2 channels are the only other voltage-dependent ion channels supposed to interact with TRIP8b (Santoro et al. 2009), we tested the expression and function of these channels in mouse brain in the following.

mRNA and protein expression of Kv1.2 in TRIP8b$^{-/-}$ mice

In a first experimental approach, we assessed the whole brain mRNA expression level of Kv1.2 in *TRIP8b*$^{-/-}$ mice in comparison to WT animals using quantitative real time PCR. Although nominally reduced expression was found for *TRIP8b*$^{-/-}$ mice, no significant differences were detected between the two genotypes (Supplementary Figure 1).

Next, protein expression of Kv1.2 channels was assessed in different brain regions by fluorescent immunohistochemistry. Kv1.2 channel protein was clearly detected in somatodendritic localizations in VB (Supplementary Figure 2A), hippocampus (Figure 1A, B) and SSC (Figure 2A) in WT, as indicated by staining a ring of plasma membrane and co-staining with the dendritic marker MAP2. The distribution profile of Kv1.2 fluorescence in the hippocampus with strong expression in the molecular layer of the dentate gyrus, in the CA3 stratum lucidum and the CA1 stratum oriens found in the present paper largely reflects published data from rat and man (Rhodes et al. 1995; Willis et al. 2018). While no significant differences in Kv1.2 fluorescence were detected in VB (Supplementary Figure 2A, B), dentate gyrus and the hippocampal CA1 region, a specific increase was found in dendritic regions of other pyramidal neurons in *TRIP8b*$^{-/-}$ mice. Kv1.2 staining in the pyramidal cell layer and stratum lucidum of the hippocampal CA3 region (Figure 1B, C) and the region of the dendritic apical trunk of cortical layer IV-V pyramidal cells (Figure 2B, C) was significantly increased in *TRIP8b*$^{-/-}$ mice.

While these findings indicate no significant differences on whole brain mRNA level and for most of the analyzed

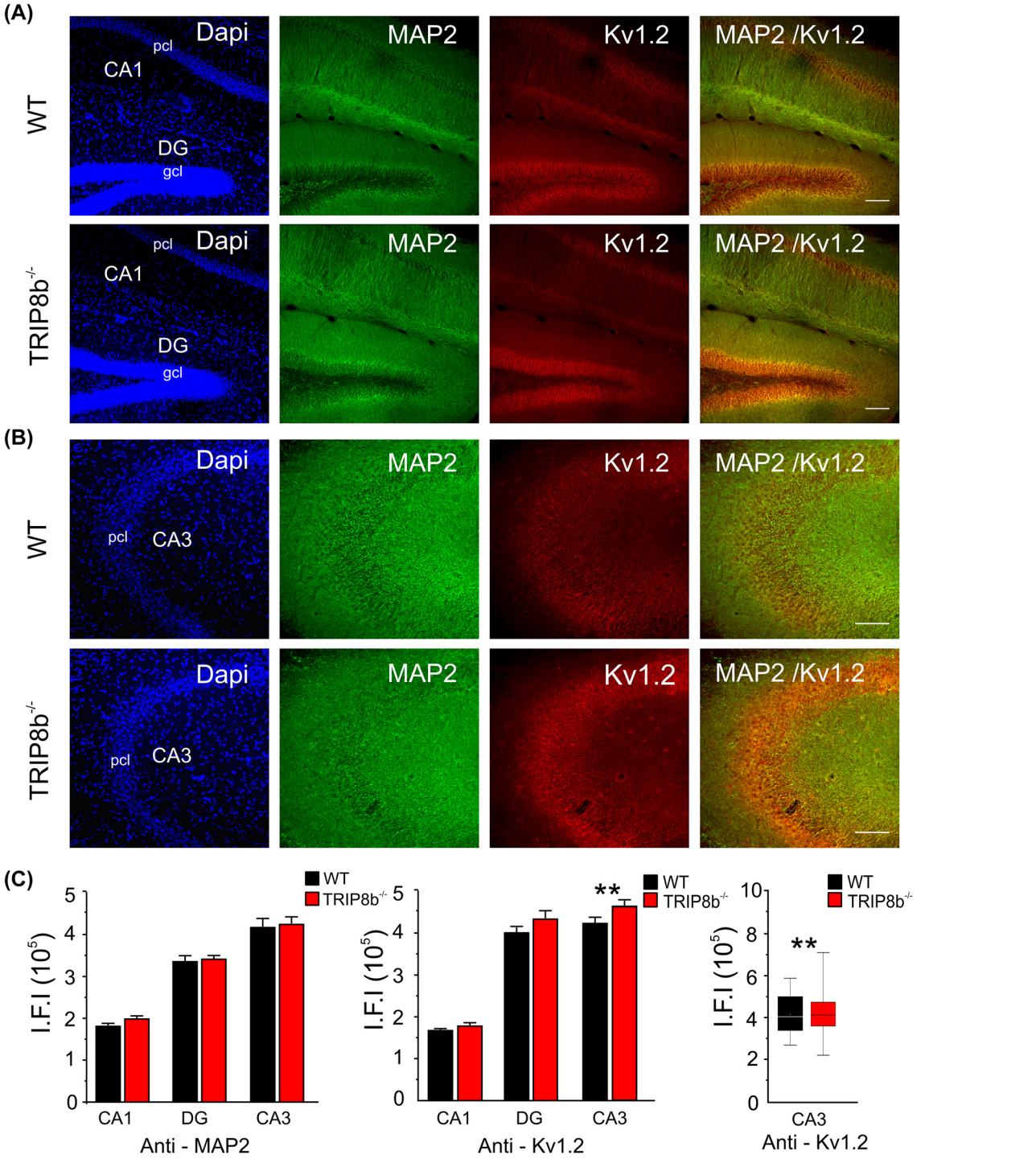

Figure 1: Expression analysis of Kv1.2 channels in the hippocampus of WT and *TRIP8b*$^{-/-}$ mice. (A and B) Immunofluorescence staining of the hippocampus (coronal sections, 40 µm) comparing the expression of MAP2 (guinea pig (gp) – anti-MAP2, 1:500) and Kv1.2 (rabbit (rb) – anti-Kv1.2, 1:500) between WT and *TRIP8b*$^{-/-}$ mice ($n = 3$ WT vs. $n = 3$ *TRIP8b*$^{-/-}$ mice, respectively). Dapi staining was used to determine cell nucleus. Note the moderate (CA1, CA3) to strong (DG) expression of Kv1.2 in the hippocampus. Scale bars indicate 100 µm. The areas cornu ammonis 1 (CA1), cornu ammonis 3 (CA3), dentate gyrus (DG), granule cell layer (gcl) and pyramidal cell layer (pcl) are indicated. Expression analysis was performed on pcl of the CA1 (A) and CA3 (B) and gcl of the DG (A). (C) Bar graphs comparing the intensity of the fluorescence signals (using integrated fluorescence intensity values) for Kv1.2 and MAP2 between WT and *TRIP8b*$^{-/-}$ mice in different hippocampal areas. A significant increase in expression of Kv1.2 was found for the CA3 area of *TRIP8b*$^{-/-}$ mice. The box plot (minimum, mean, median line, maximum) emphasizes the significant difference.

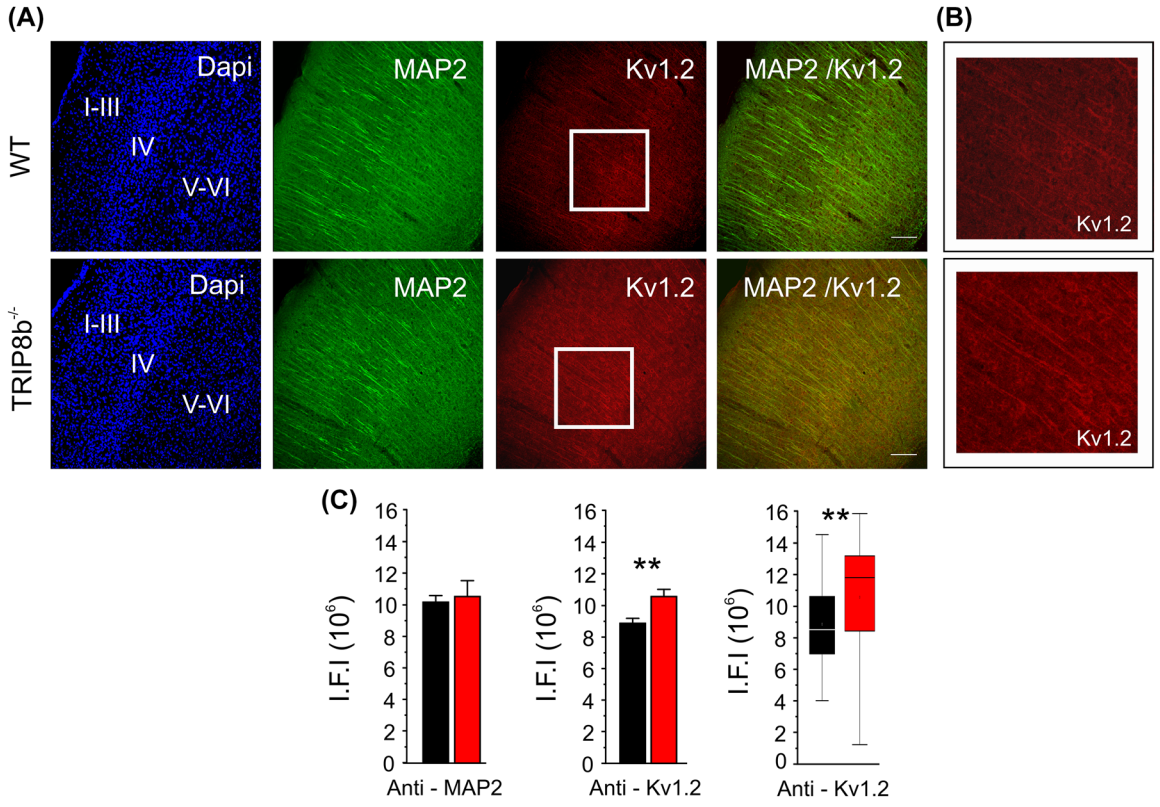

Figure 2: Expression analysis of Kv1.2 channels in the neocortex of WT and *TRIP8b*$^{-/-}$ mice. Immunofluorescence staining of the somatosensory cortex (SSC, coronal sections, 40 µm) comparing the expression of MAP2 (guinea pig (gp) – anti-MAP2, 1:500,) and Kv1.2 (rabbit (rb) – anti-Kv1.2, 1:500) between WT and *TRIP8b*$^{-/-}$ mice (n = 3 WT vs. n = 3 *TRIP8b*$^{-/-}$ mice, respectively). Expression analysis was performed on cortical layers IV-V. Scale bars indicate 100 µm. (B) Enlarged image showing Kv1.2 expression of the areas defined by the white boxes in (A). Apical dendrites are clearly stained in *TRIP8b*$^{-/-}$ mice (lower panel). (C) Bar graphs comparing the intensity of the fluorescence signals (using integrated fluorescence intensity values) for Kv1.2 and MAP2 between WT and *TRIP8b*$^{-/-}$ mice in SSC. A significant increase in expression was found for Kv1.2 in the SSC of *TRIP8b*$^{-/-}$ mice. The box plot (minimum, mean, median line, maximum) emphasizes the significant difference.

brain areas on protein level, there is a specific increase and dispersion for two cortical structures. This may indicate that Kv1.2 localization in distinct neuronal compartments is less restricted in the absence of TRIP8b.

Pharmacological characterization of Kv1.2-mediated outward current

We used Psora-4, a potent Kv1.x selective channel blocker before to characterize native K^+ currents with contributions by Kv1.2 channels (Decher et al. 2010). In addition, we here used TsTX-Kα, a scorpion toxin with high affinity to Kv1.2 and Kv1.3, but not Kv1.1 and Kv1.4 containing channels (Hopkins 1998; Rodrigues et al. 2003; Werkman et al. 1993). To elicit K^+ outward currents, acutely isolated neurons were held at a potential of −69 mV and hyperpolarized to a conditioning potential of −109 mV (duration, 2 s) before stepping to various test potentials (−69 to +81 mV; 30 mV increment; 2 s duration; see Figure 3 inset). Since cell morphology seems to influence the electrophysiological properties of hippocampal CA3 pyramidal cells in particular (Krichmar et al. 2002), these neurons were recorded in brain slices. In order to increase cell stability and to focus on a voltage range typical for Kv1-like (D-type) K^+ channels in hippocampal neurons (Xiao et al. 2021), the voltage protocol was modified in these recordings (depolarizing steps from −59 to +41 mV; 10 mV increment; see Supplementary Figure 3). Our voltage protocols evoked typical voltage-dependent K^+ currents (Figure 3A, B; Supplementary Figure 3) described earlier in hippocampus and thalamus (Budde et al. 1992; Decher et al. 2010). When the peak outward current at maximal depolarization was analyzed (closed circles in Figure 3A and Supplementary Figure 3), significantly higher amplitudes were found in SSC pyramidal cells of *TRIP8b*$^{-/-}$ mice (WT: 8537 ± 249 pA, n = 36; *TRIP8b*$^{-/-}$: 9501 ± 335 pA, n = 29; $P < 0.05$; Figure 3C). No differences were found in CA1 pyramidal cells (WT: 8448 ± 415 pA, n = 26; *TRIP8b*$^{-/-}$: 8775 ± 429 pA, n = 30),

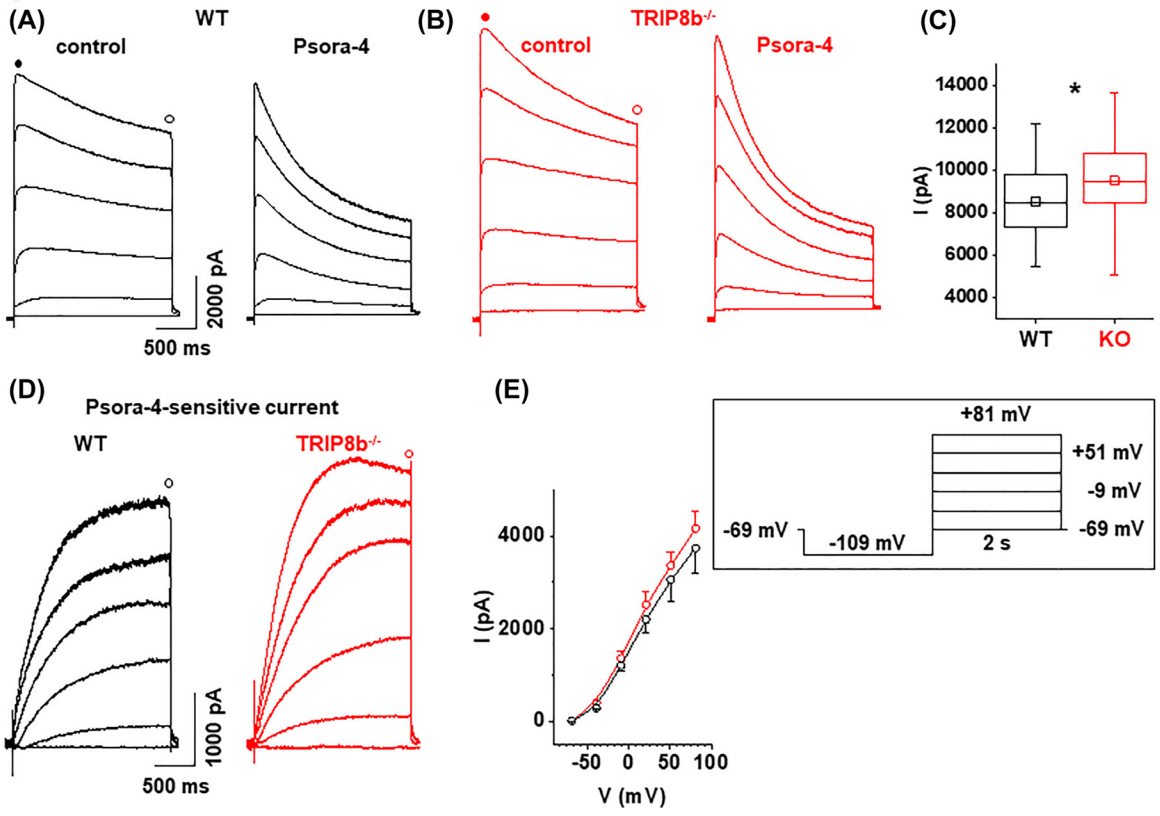

Figure 3: Outward currents in acutely isolated SSC pyramidal cells from WT and *TRIP8b*$^{-/-}$ mice. (A and B) Families of outward currents evoked by depolarizing voltage steps. The voltage protocol is indicated in the inset. The depolarizing steps varied between −69 and +81 mV (Δ*V* = 30 mV). Voltage-activated outward currents recorded under control conditions (left panels) and in the presence of Psora-4 (right panels) are shown for WT (A) and *TRIP8b*$^{-/-}$ (B) mice. Points in time for obtaining peak and late current amplitudes for further analysis are indicated by closed and open circles, respectively. (C) Box plot (minimum, mean, median line, maximum) of peak current amplitudes in neurons from WT (black) and *TRIP8b*$^{-/-}$ (red) mice. A significant difference was found between the genotypes. (D) Psora-4-sensitive current components, as difference between the currents measured before and after application of Psora-4 are shown for WT (black traces) and *TRIP8b*$^{-/-}$ (red traces) mice. The point in time for obtaining the late current amplitude for further analysis is indicated by open circles. (E) Late current amplitudes of the blocker-sensitive currents were obtained and plotted against the depolarizing step potentials. Typical outwardly rectifying K^+ current-voltage (I–V) plots were obtained for SSC pyramidal cells from WT (black open circles; *n* = 6) and *TRIP8b*$^{-/-}$ (red open circles; *n* = 6) mice.

CA3 pyramidal cells (WT: 4827 ± 678 pA, *n* = 11; *TRIP8b*$^{-/-}$: 4526 ± 862 pA,-*n* = 11) and VB TC neurons (WT: 9023 ± 317 pA, *n* = 21; *TRIP8b*$^{-/-}$: 9252 ± 305 pA, *n* = 22).

Next, we used 100 nM Psora-4, a concentration sufficient to completely block all members of the Kv1 family (Decher et al. 2010; Vennekamp et al. 2004) in different acutely isolated neuronal cell types (hippocampal CA1 pyramidal cells; SSC pyramidal cells; VB TC neurons) and neurons in brain slices (hippocampal CA3 pyramidal cells). Since we observed changes in protein expression and net outward current in SSC, we recorded these cells at first (Figure 3A, B). In neurons from WT (Figure 3A) and *TRIP8b*$^{-/-}$ (Figure 3B) mice, Psora-4 reduced outward currents over the complete investigated voltage range. Peak (closed circles in Figure 3A, B) and late (open circle in Figure 3A, B) current components were weakly and strongly affected respectively, thereby pointing to a Psora-4-resistant component of Kv1.x currents in SSC. The blocker-sensitive currents that were obtained by graphical subtraction of currents recorded under control conditions and in the presence of the Kv channel blocker revealed slow activation kinetics and inactivated moderately during the induced voltage step (Figure 3D). Although nominally higher amplitudes were found in *TRIP8b*$^{-/-}$ mice (Figure 3E) no significant differences were obtained.

Next, we assessed the degree of inactivation of the Psora-4-sensitive current component (Figure 4). While WT neurons revealed some variability in the degree of inactivation in all cell types, this parameter was less scattered in neurons from *TRIP8b*$^{-/-}$ mice. Significant differences were found for SSC pyramidal cells (Figure 4A) and CA1 pyramidal cells (Figure 4B) but not for VB TC neurons (Figure 4C) and CA3 pyramidal cells (Figure 4B) when the voltage step to +81 mV (to +41 mV in CA3 pyramidal cells) was compared between genotypes.

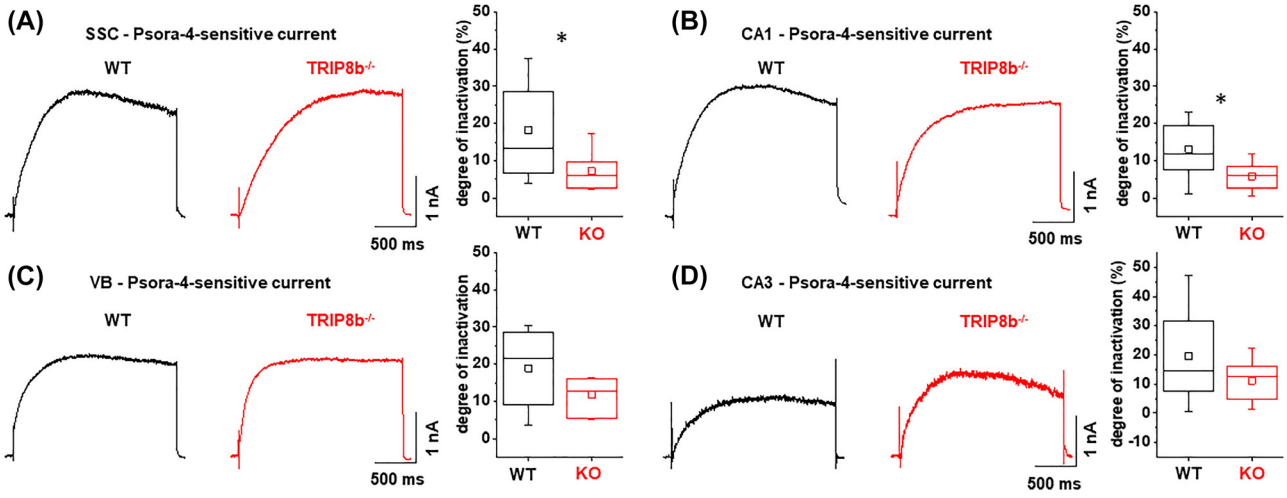

Figure 4: Inactivation of blocker-sensitive currents recorded from neurons following acute isolation (CA1, SSC, VB) and from brain slices (CA3) from WT and *TRIP8b*$^{-/-}$ mice. (A–D) Psora-4-sensitive current component, as difference between the currents measured before and after application of Psora-4 in SSC pyramidal cells (A), CA1 pyramidal cells (B), VB TC neurons (C) and CA3 pyramidal cells (D). Currents from WT (black traces) and *TRIP8b*$^{-/-}$ (red traces) were evoked by depolarizing steps to +81 mV and +41 mV for isolated neurons (A–C) and cells in brain slices (D), respectively. Box plots (minimum, mean, median line, maximum) of the degree of inactivation in neurons from WT (black; SSC, $n = 9$; CA1, $n = 8$; VB, $n = 6$; CA3, $n = 11$) and *TRIP8b*$^{-/-}$ (red; SSC, $n = 7$; CA1, $n = 8$; VB, $n = 7$; CA3, $n = 11$) mice. Significant differences were found between the genotypes for SSC and CA1.

In order to allow further comparison between WT and *TRIP8b*$^{-/-}$ mice, we assessed the percentage current reduction in the following. In order to allow the use-dependent block of Psora-4 (Decher et al. 2010; Vennekamp et al. 2004), outward currents were repetitively activated until the maximal block was achieved (Supplementary Figure 4A). Psora-4 had a differential blocking effect in the investigated brain regions that was strongest in pyramidal cells in the CA1 region (Supplementary Figure 4B). However, no significant differences were found in SSC pyramidal cells, CA1 pyramidal cells, VB TC neurons and CA3 pyramidal cells (Figure 4B) when the voltage step to +81 mV (to +41 mV in CA3 pyramidal cells) was compared between genotypes.

Next, TsTX-Kα (100 nM) that specifically blocks Kv1.2 and Kv1.3 channels was used (Hopkins 1998; Werkman et al. 1993). As expected, the effect of the scorpion toxin was smaller compared to the Psora-4-induced reduction. In acutely isolated neurons, TsTX-Kα reduced the early (hippocampus CA1: 14.3%; SSC: 17.0%; VB: 10.4%) and late (hippocampus CA1: 30.8%; SSC: 22.5%; VB: 20.9%) component at +81 mV by a different degree. Again, currents generated by hippocampal CA1 neurons were less resistant to blocker application compared to SSC and VB neurons. When the voltage step to +81 mV was compared between genotypes, there were no significant differences in CA1 pyramidal cells (Supplementary Figure 5A), VB TC neurons (Supplementary Figure 5B) and SSC pyramidal cells (Supplementary Figure 5C).

These findings indicate no significant differences of the effects of two substances blocking outward currents with Kv1.2 contribution, thereby pointing to unaltered Kv1.2 channel function in *TRIP8b*$^{-/-}$ mice.

Co-expression of Kv1.2 channels and TRIP8b in oocytes

To assess the interaction between Kv1.2 and TRIP8b more directly, both membrane proteins were expressed in oocytes in equal amounts. In the experiments presented here, no effects on Kv1.2 current amplitudes upon co-expression with TRIP8b were detected. Channels were activated by voltage steps (2 s duration) ranging from –120 to +60 mV in 20 mV increments. The resulting currents revealed no differences in maximal amplitude when compared between oocytes expressing Kv1.2 alone (12.3 ± 1.3 µA; $n = 16$) or in combination with TRIP8b (13.6 ± 0.4 µA; $n = 23$; Figure 5A). In addition, no differences were found when channels were activated by a constant depolarizing voltage step to +60 mV and deactivating tail currents were evaluated (Figure 5B). These findings do not support a direct influence of TRIP8b on the amplitude of the current through Kv1.2 channels.

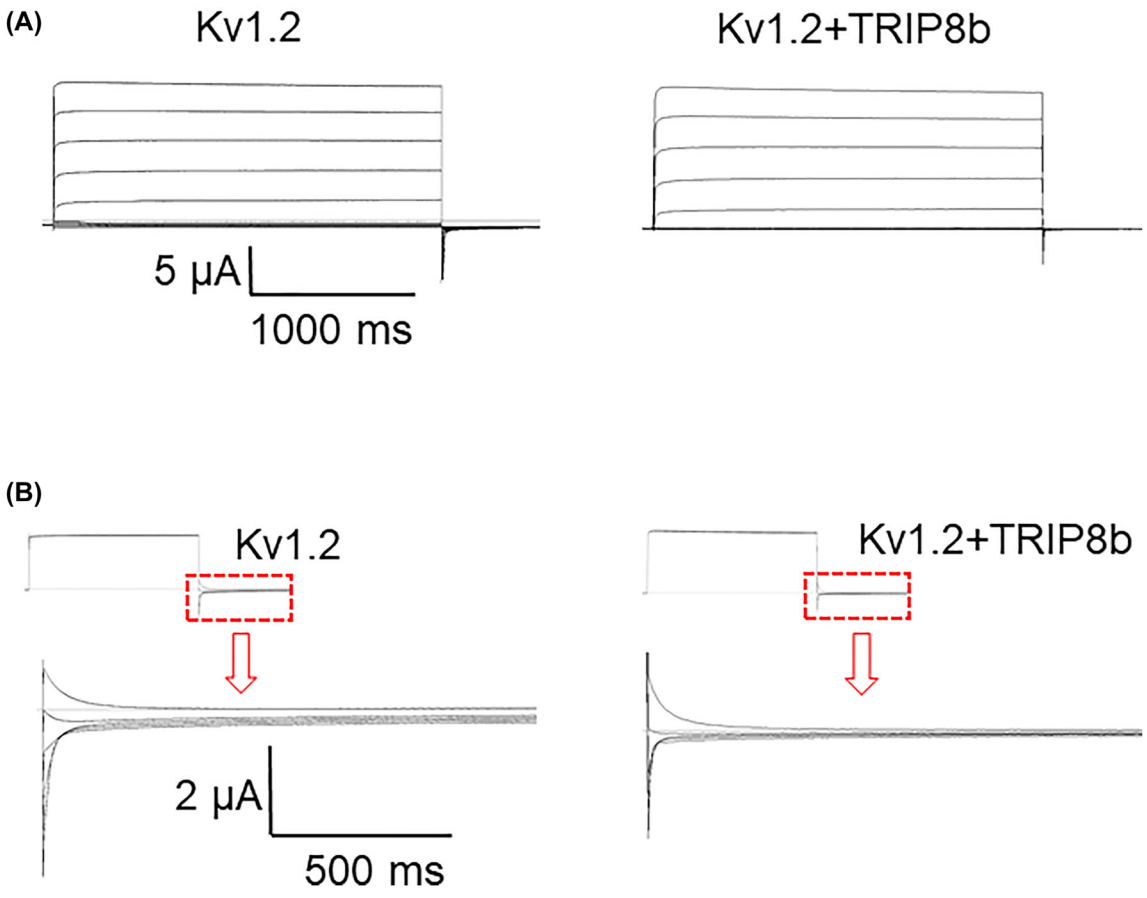

Figure 5: Co-expression of TRIP8b with Kv1.2 does not induce prominent changes in Kv1.2 channel current amplitude. (A) Kv1.2 was expressed alone or co-expressed with TRIP8b in *Xenopus laevis* oocytes. Channels were activated by 2 s pulses from −120 mV to +60 mV in 20 mV increments. Current–voltage relationship for Kv1.2 expressing oocytes in absence and presence of TRIP8b were recorded and representative currents are depicted. Zero current is indicated by a light grey line. (B) Deactivating currents were recorded at voltages of −40, −60, −80 and −100 mV following activation by a constant pulse to +60 mV (n = 15–23). Non-injected oocytes or injection of TRIP8b without Kv1.2 produced no currents (n = 10). Zero current is indicated by a light grey line.

Effects of TsTX-Kα on action potential firing in thalamic neurons

Next, TsTX-Kα was applied to VB TC neurons in brain slices. Under current clamp conditions, depolarizing current pulses of increasing amplitude were applied from RMP (66.0 ± 0.7 mV; n = 7) in WT animals. Application of TsTX-Kα induced a significant (P < 0.05) depolarization of the RMP (63.2 ± 0.9 mV; n = 7). The number of APs in response to increasing depolarization was significantly increased in the presence of the scorpion toxin (F (21,126) = 4.630, P < 0.001, Figure 6A). Pairwise comparisons of the number of APs showed significant differences for depolarizing current steps between +110 and +330 pA. In addition, the number of APs riding on top of a rebound low-threshold Ca^{2+} spike was nominally increased, but the increase was only marginally significant (Figure 6B). Nevertheless, in 4 out of 7 TC neurons TsTX-Kα application was associated with the appearance of increased synaptic activity and spontaneous bursting, thereby indicating enhanced neuronal excitability.

Discussion

Our results suggest that the RNA expression and function of Kv1.2 channels is not significantly altered in *TRIP8b*$^{-/-}$ mice compared to WT animals. The experimental evidence supporting this idea can be summarized as follows: (1) Quantitative real time PCR analysis revealed no difference in whole brain mRNA expression between WT and *TRIP8b*$^{-/-}$ mice. (2) Analyses of fluorescent staining intensity revealed no difference in protein expression levels between WT and *TRIP8b*$^{-/-}$ mice in VB. In hippocampus and cerebral cortex, Kv1.2 expression was increased. However, this increase occurred in locations revealing low expression in WT mice. (3) In whole cell patch-clamp experiments, two compounds

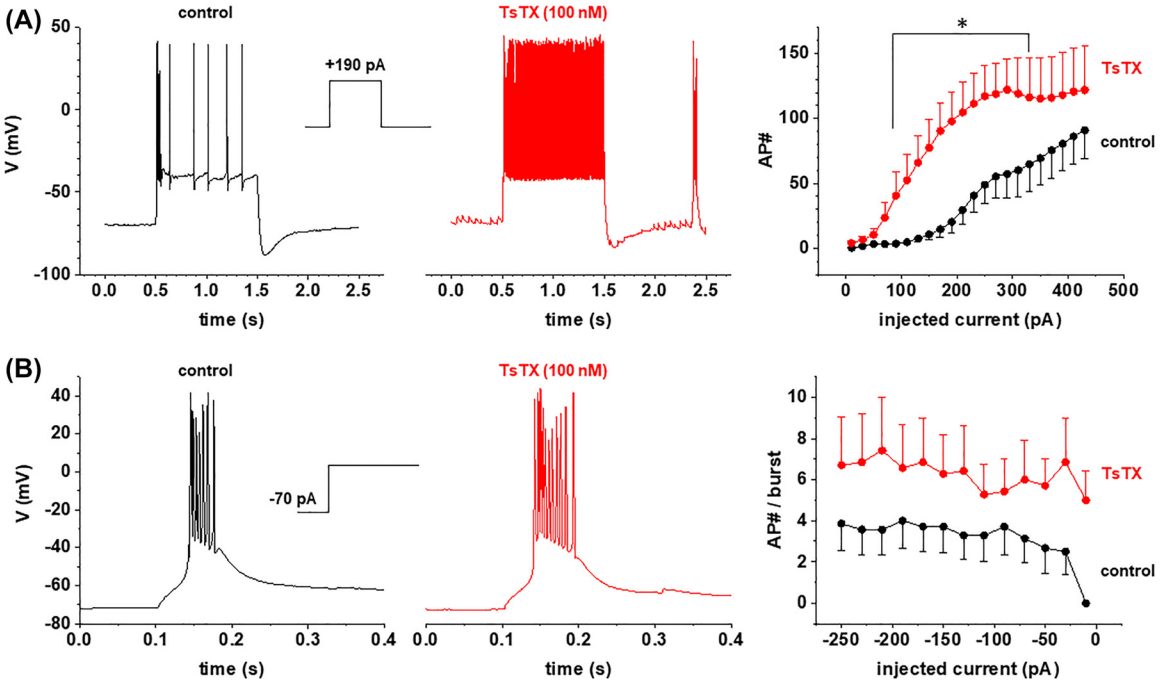

Figure 6: Changes in firing pattern of TC neurons in WT mice following application of TsTX. (A) Sample traces recorded in response to the injection of depolarizing currents (+190 pA) from the RMP of TC neurons in the VB complex of WT mice under control conditions (black; $n = 7$) and in the presence of TsTX (red; $n = 7$). The number of APs elicited by the injection of positive currents with 20 pA increments from RMP is shown. Significantly (repeated-measures ANOVA, $P < 0.001$) more APs were evoked in the presence of TsTX. Note the occurrence of a spontaneous burst in the presence of the blocker. (B) Sample traces of rebound bursting elicited by hyperpolarizing current pulse (−70 pA) from RMP. The number of APs in a burst was different between control conditions and presence of TsTX for some of the hyperpolarizing steps.

blocking Kv1.2 channels revealed no differences in the potency of blocking K^+ outward currents in four different brain regions. (4) Heterologous expression of Kv1.2 channels revealed no differences in current amplitude in the presence and absence of TRIP8b. Furthermore, challenging VB TC neurons with TsTX-Kα in current clamp experiments increased AP firing, an effect that was opposite to the knockout of TRIP8b. Therefore, we conclude that a TRIP8b-dependent alteration of Kv1.2 channels is unlikely to contribute to the changes in AP firing found in *TRIP8b*$^{-/-}$ mice. Nevertheless, Kv1.2 channels effectively control tonic AP firing in TC neurons. Furthermore, loss of TRIP8b seems to indirectly influence the properties of early activating Kv channels in some brain regions and seems to contribute to the degree of inactivation of the Psora-4-sensitive component.

Influence of HCN channels on action potential firing in TC neurons

While HCN channels directly influence pacemaker potentials and LTS amplitude, their operational voltage range is less suited to influence tonic AP firing at depolarized membrane potentials (He et al. 2014). Nevertheless, by setting RMP and R_{input} these channels may shape tonic firing pattern. Indeed, ambiguous effects of decreased HCN channel availability have been reported. In *HCN4*$^{-/-}$ mice, I_h current in VB TC neurons was reduced by about 58% (Zobeiri et al. 2019). In these neurons, application of depolarizing current steps from a depolarized membrane potential (−55 mV) induced more APs compared to WT mice. In *TRIP8b*$^{-/-}$ mice, I_h current in VB TC neurons was reduced by about 80% (Zobeiri et al. 2018). In these neurons, application of depolarizing current steps from a depolarized membrane potential (−60 mV) induced less tonic APs compared to WT mice. Furthermore, the increase (about 14%) and decrease (about 19%) of I_h current amplitudes by IL-1β and INF-α were associated with increased and decreased firing of APs following application of depolarizing current steps from RMP (Oniani et al. 2022). These findings allow no clear-cut conclusion concerning the influence of HCN channel activity on tonic firing in TC neurons. Additional cellular and network properties may have been altered in the particular recording conditions (altered GABAergic inhibition in HCN4$^{-/-}$ mice; altered Kv channel function and lowered cAMP levels in *TRIP8b*$^{-/-}$ mice; modulation of multiple ion channels by cytokines).

Expression of Kv1.2 channels in the thalamus

Electrophysiological (voltage-dependent properties), pharmacological (sensitivity to blockers) and molecular biological (PCR, gene knockout) strategies have been used before to assess the expression of Kv1 channels in rodent TC neurons from different nuclei (Decher et al. 2010; Kanyshkova et al. 2011; Kasten et al. 2007). In rats, the expression of Kv1.1, Kv1.2, Kv1.4, Kv1.6, and to a lesser extent Kv1.3, and Kv1.5 was found. This expression profile was in agreement with the blocking effects of Hongotoxin-1 ($HgTX_1$; blocks Kv1.1, Kv.1.2, Kv1.3 or Kv1.6) and Psora-4 on rat TC neuron outward currents. Interestingly, the blocking effect of Psora-4 was stronger in hippocampal CA1 pyramidal neurons compared to dorsolateral geniculate nucleus (dLGN) TC neurons. In the present study, we present very similar findings for mice with Psora-4 and TsTX-Kα revealing stronger outward current reduction in hippocampal CA1 pyramidal neurons compared to VB TC neurons. Although none of the used substances solely blocks Kv1.2 channels, the functional expression of these channels is very likely. Based on the effect of TsTX-Kα on the firing properties of VB neurons found here, Kv1.2 channels strongly control TC neuron excitability by limiting AP firing. This finding is in good agreement with the increasing effect of α-dendrotoxin (α-DTX), a blocker of Kv1.1, Kv1.2 and Kv1.6, on AP firing in mouse TC neurons of the lateral dorsal thalamic nucleus (Kasten et al. 2007). Therefore it is not surprising that Kv1.2 knockout mice reveal an epileptic phenotype (Robbins and Tempel 2012). The adenovirus-associated overexpression of Kv1.2 channels in the CM thalamus was associated with reduced tonic firing in TC neurons (Cazzin et al. 2011), thereby mirroring our results using a Kv1.2 channel blocker. Importantly, neither Kv1.2 channel overexpression nor Kv1.2 channel block (present study) strongly influence burst activity in TC neurons. On the behavioral level, Kv1.2 overexpression was associated with a decrease in the pro-arousal effect of caffeine in rats (Cazzin et al. 2011). The latter is in good agreement with the demonstration that the microinfusion of an antibody directed against Kv1.2 channels into the CM thalamus restores consciousness in anaesthetized rats (Alkire et al. 2009). Therefore, our findings clearly support the view that Kv1.2 channels control tonic activity in rodent TC neurons.

TRIP8b interaction with ion channels

The modulation of HCN channel properties and expression pattern by TRIP8b is well established (Han et al. 2020). The only significant effect on expression levels with any of the TRIP8b isoforms on ion channels other than HCN channels was an about 15% increase in Kv1.2 current amplitude upon co-expression with the TRIP8b (1a-4) isoform (Santoro et al. 2009). In the present study, no increase in Kv1.2 amplitude was found upon co-expression of both proteins. While the reason for the discrepancies in expression systems is unknown (e.g., different expression vectors were used), the very similar effects of Kv1.2 blocking compounds argue against an increasing effect in native neurons. Nevertheless, our immunofluorescent approach revealed increased fluorescence in some specific locations in the brain. Kv1.2 staining in the absence of TRIP8b was increased in the pyramidal cell layer and stratum lucidum of the hippocampal CA3 region and in the apical trunk of cortical layer IV-V pyramidal cells. In rodent as well as in human brain, the expression of Kv1.2 is normally moderate in the somatodendritic compartment, while it is prominent in the axonal compartment (Rhodes et al. 1995; Sánchez-Ponce et al. 2012; Willis et al. 2018). We conclude that TRIP8b may help to direct Kv1.2 channels to the plasma membrane in defined neuronal compartments thereby influencing ion channel and current densities. The loss of TRIP8b results in a wider expression range.

We found that the degree of inactivation of the Psora-4-senstive component was stronger in the absence of TRIP8b. These findings indicate that TRIP8b, like other ion channel β subunits may contribute to the complex process of Kv1 channel inactivation (Yee et al. 2022). It has been observed before that the time-dependent inactivation of Psora-4-sensitive current component in different native neurons is rather moderate (Decher et al. 2010). However, the differential expression and association of cytoplasmic β subunits with pore-forming α subunits as well as the influence of membrane lipids and cellular metabolites may contribute significantly to the complexity and heterogeneity of time-dependent inactivation of individual native K^+ currents (Zemel et al. 2018). In addition, there seems to be a compensatory upregulation of other Kv channels in the TC system in the absence of TRIP8b that may help to counteract the cortical over-excitability found in *TRIP8b*$^{-/-}$ mice (Heuermann et al. 2016). In VB TC neurons an increased availability of an A-type K^+ current that is probably based on Kv4 channels was found (Kanyshkova et al. 2011; Zobeiri et al. 2018). In the present study, Kv channels contributing to the early peak outward current revealed increased activity in SSC pyramidal cells. Therefore, in two cell types essential for the generation of epileptic SWDs a compensatory upregulation of Kv channel activity was found when TRIP8b was knocked out that probably reduced the occurrence of seizures during the history of this mutant mouse line. In general, our findings support the view that TRIP8b directly or indirectly interacts with different Kv channels thereby

adding to the functional profile of this auxiliary ion channel subunit. The molecular mechanisms behind these findings will be assessed in future studies.

Materials and methods

Preparation of acute brain slices and whole-cell recording

Four to six weeks old *C57BL/6J* mice were decapitated according to effective legal standards without anesthesia using DecapiCones (Braintree Scientific Inc., Braintree, MA 02185, USA) and brain tissue was rapidly removed from the skull and placed in an ice-cold oxygenated slicing solution containing (in mM): sucrose, 234; glucose, 11; NaH_2PO_4, 24; $MgSO_4$, 10; and $CaCl_2$, 0.5. Brain slices (250 µm) containing the VB were prepared. Slices were transferred to and kept in a chamber with artificial cerebrospinal fluid (ACSF) containing (in mM): NaCl, 120; KCl, 2.5; NaH_2PO_4, 1.25; $NaHCO_3$, 22; $MgSO_4$, 2; $CaCl_2$, 2; glucose, 25. Temperature was set to 33 °C for 30 min and slices were allowed to cool down to room temperature. pH was adjusted to 7.35 by bubbling with carbogen (95% O_2 and 5% CO_2).

For slice recordings, patch pipettes were pulled from borosilicate glass (GC150T-10; Clark Electromedical Instruments, Pangbourne, UK) and had a resistance of 2–3 MΩ; typical access resistance was in the range of 4–10 MΩ. Series resistance compensation of >30% was routinely applied. Patch clamp experiments with an EPC-10 amplifier (E.S.F. electronics) were controlled by PatchMaster software. Data were corrected for liquid junction potential.

For voltage clamp recordings in CA3 pyramidal cells in brain slices, the bath temperature was set to 33 ± 0.5 °C and the extracellular solution contained (mM): NaCl, 130; KCl, 2; $NaHCO_3$, 22; $C_6H_{12}O_6$, 10; $CaCl_2$, 0.5; $MgCl_2$, 3.5. The intracellular solution contained (mM): NaCl, 10; KCl, 10; K-Gluconate, 85; K_3-Citrate, 20; HEPES, 10; K-BAPTA, 3; Mg-ATP, 3; Na-GTP, 0.5; Phosphocreatine, 15; $CaCl_2$, 0.5; $MgCl_2$, 1. For analysis of K^+ currents, cells were held at a potential of −69 mV and hyperpolarized to a conditioning potential of −109 mV (duration, 2 s) before stepping to various test potentials (−59 to +41 mV; 10 mV increment; 2 s duration). Outward currents of CA3 pyramidal cells were compared before and after application of 100 nM Psora-4 (Sigma).

Current clamp recordings in VB TC neurons in brain slices were carried out in ACSF at the temperature of 33 ± 0.5°C. The internal pipette solution contained (in mM): K-gluconate, 88; K_3-citrate, 20; NaCl, 10; HEPES, 10; $MgCl_2$, 1; $CaCl_2$, 0.5; BAPTA, 3; Mg-ATP, 3; Na_2-GTP, 0.5 phosphocreatin, 15 with a pH of 7.25 and an osmolarity of 290–300 mOsmol/kg. The firing pattern and membrane properties of VB TC neurons were compared before and after application of 100 nM TsTX-Kα (Alomone Labs) using a current-clamp recording protocol consisting of a series of hyperpolarizing and depolarizing current injections (−250 to +430 pA, 1 s duration) with 20 pA increments, from the RMP.

Acute isolation of hippocampal, thalamic and cortical neurons

Preparation of coronal brain slices for acute isolation was done as described above. The CA1 region of the hippocampus, VB and SSC were visually identified in 500 µm coronal slices of 4–8 weeks old *TRP8b*$^{-/-}$ and *C57BL/6J* mice, dissected, and transferred to a spinner flask with cold (5 °C) and oxygenated dissociation solution containing (mM): NaCl, 120; KCl, 5; $MgCl_2$, 3; $CaCl_2$, 1; PIPES, 20; glucose, 14; pH, 7.3–7.4. The solution was warmed up to 30 °C and then trypsin (1 mg/mL) was added. Slices were incubated for another 30–40 min in the trypsin containing solution and thereafter washed three times in trypsin-free oxygenated dissociation solution and kept there for 10 min. Dissociation of single neurons was achieved by triturating a slice in low Ca^{2+} (0.2 mM) dissociation solution with fire-polished Pasteur pipettes.

Whole cell voltage-clamp recordings in isolated neurons

Whole-cell recordings were performed on visually identified TC neurons and pyramidal cells at controlled room temperature (20–22 °C). Borosilicate glass pipettes with a resistance of 3–5 MΩ were used; typical access resistance was in the range of 4–10 MΩ. Series resistance compensation of >30% was routinely applied. Voltage clamp experiments with an EPC-10 amplifier (E.S.F. electronics) were controlled by PatchMaster software. For voltage clamp recordings, the extracellular solution contained (mM): NaCl, 140; KCl, 2; HEPES, 10; dextrose, 10; $MgCl_2$, 3; $CaCl_2$, 1; TTX, 0.001; $CdCl_2$, 0.15; pH 7.35 and 305 mOsm. The intracellular solution contained (mm): K-gluconate, 85; K_3-citrate, 10; NaCl, 10; KCl, 10; K-BAPTA, 3; $CaCl_2$, 0.5; $MgCl_2$, 1; HEPES, 10; MgATP, 3; Na_2GTP, 0.5; phosphocreatine, 15; pH 7.25 and 295 mOsm. Data were corrected for liquid junction potential. For analysis of K^+ currents, cells were held at a potential of −69 mV and hyperpolarized to a conditioning potential of −109 mV (duration, 2 s) before stepping to various test potentials (−69 to +81 mV; 30 mV increment; 2 s duration). Outward currents of neurons were compared before and after application of 100 nM Psora-4 or 100 nM TsTX-Kα.

Analysis of the Psora-4-sensitive current component

During wash in of Psora-4, cells were depolarized every 20 s to +41/+81 mV to monitor the use-dependent current block (Supplementary Figure 4A). Maximal block was usually achieved after 4–8 pulses. The degree of time-dependent inactivation of the Psora-4-sensitive current was obtained by dividing the current amplitude at the end of the depolarizing pulse by the peak current amplitude and calculating the percentage reduction.

Oocyte expression

Xenopus laevis oocytes were obtained by *Ecocyte* (Dortmund, Germany). Linearized cDNA was transcribed using the *mMessage mMachine* kit (Ambion) and the constructs were expressed in oocytes by injection of 5 ng Kv1.2 or TRIP8b cRNA. Oocytes were kept in a Barth solution containing (in mM) NaCl, 90; HEPES, 10; KCl, 2; $MgCl_2$, 1; $CaCl_2$, 1; pH 7.5, for 3 days at 18 °C. Whole-cell currents in *X. laevis* oocytes were recorded at room temperature as described before (Strutz-Seebohm et al. 2007). In brief, two-electrode voltage clamp (TEVC) was applied using a *Turbo Tec 10CD* amplifier (NPI Electronic GmbH, Tamm, Germany) and an *NI USB 6221* interface (National instruments, USA) combined with *GePulse* software (Michael Pusch, Genova, Italy). Recording pipettes pulled from borosilicate glass were filled with 3 M KCl and had resistances of 0.5–1 MΩ. Recordings were performed in ND96 solution containing

(in mM) NaCl, 96; KCl, 4; $CaCl_2$, 1; $MgCl_2$, 1.8; HEPES, 5; pH 7.2–7.4. Data analysis was conducted by *ANA* software (Michael Pusch, Genova, Italy).

Molecular biology – cloning

The cDNA encoding rat TRIP8b is based on database entry NM_173152.1 but differs by one residue (N335D). The cDNA was individually subcloned into pBF1 oocyte expression vector for synthesizing cRNA used in the voltage clamp system. The construct was confirmed by DNA sequencing of the entire gene (Seqlab Company).

Quantitative RT-PCR

Whole brain was obtained from 10 to 12 weeks old *C57BL/6J* and *TRIP8b*$^{-/-}$ mice and mechanically homogenized. RNA was then isolated using QIAzol lysis reagent (QIAGEN) following the standard procedures. cDNA synthesized by using manufacturer's protocol with random hexamer primers (Roche). Thereafter, cDNA was used to run quantitative polymerase chain reaction (qPCR) with fluorescein amidites-labeled Taqman primers for *Kcna2* (Mm01197194_m1, ThermoFisher Scientific). GAPDH (Mm99999915_g1, ThermoFisher Scientific) was used as a reference gene for normalization of our interest gene's expression level. qPCR was performed for 40 cycles at 95 °C for 15 s and 60 °C for 1 min, and sample reactions were measured as triplicates. Data were calculated using the changes in cycle threshold (ΔCt = Ct (gene of interest) – Ct (reference gene)) and relative expression levels were specified using the $2^{-\Delta\Delta Ct}$ method. Results are expressed as percentage.

Immunofluorescence staining

Mice were anesthetized by inhalation anesthesia (Isoflurane, 5% in O_2; CP Pharma, Germany) and perfused transcardially with phosphate-buffered saline (PBS) and 4% paraformaldehyde (PFA). Brains were removed and post-fixed for 2 h in 4% PFA and later in 30% sucrose for 48–72 h. Free-floating horizontal sections (40 µm) were cut and stored at –20 °C in cryoprotectant solution. Sections were washed three times for 10 min in PBS and incubated for 2 h in blocking solution (10% normal goat serum, 3% BSA, 0.3% Triton-X100 in PBS) followed overnight incubation at 4 °C with the following primary antibodies: polyclonal rabbit (rb)-anti-Kv1.2 (1:500, Alomone Labs) and polyclonal guinea pig (gp)-anti-MAP2 antibodies (1:500; Synaptic Systems). After incubation with the primary antibodies, slices were washed three times for 10 min in PBS and transferred to the secondary antibody solution (Alexa Fluor 594 gt-anti-rb-IgG, 1:1000 and Alexa Fluor 488 gt-anti-gp-IgG, 1:500) for 90 min, washed three times for 10 min and mounted with a mounting medium (VECTASHIELD with DAPI, Vector Laboratories Inc., Burlingame, CA, USA) for confocal microscopy. For quantification of immunofluorescence staining, the SSC, hippocampus and VB were visually identified in coronal brain slices (3 slices per animal). Regions of interest (ROI) were manually assigned and analyzed using laser scanning confocal microscopy (Nikon eC1 plus). Staining was quantified by using ImageJ software (NIH) as integrated fluorescence intensity (I.F.I) of all pixels in each ROI.

Statistics

All data are expressed as the mean ± standard error of the mean. We used the Shapiro-Wilk-test to prove normality of our data. Student's *t*-tests were used for simple comparison between groups. In case of multiple comparisons, repeated-measures ANOVAs were used for analyses. Mauchly's test of sphericity was used for the repeated-measures ANOVA. Where sphericity assumption was violated ($P < 0.05$), the Greenhouse–Geisser correction was applied. Student's *t*-test was used as post hoc test. The data analysis was performed using IBM SPSS Statistic for Windows, Version 28.0 (Armonk, NY: IBM Corp.) and Origin (Pro), Version 2020b (OriginLab Corporation, Northampton, MA, USA). CorelDRAW Graphics Suite X8 was used for figure plotting. Differences were considered statistically significant if *P* values were <0.05; *, **, and *** indicate $P < 0.05$, $P < 0.01$, and $P < 0.001$, respectively.

Acknowledgments: The authors thank Elke Naß, Alexandra Markovic, Katrin Foraita and Julia Kollmann for excellent technical assistance. This work was supported by DFG (GRK 2515 to GS and TB; BU1019/16-1 to TB).

Author contributions: All the authors have accepted responsibility for the entire content of this submitted manuscript and approved submission.

Research funding: None declared.

Conflict of interest statement: The authors declare no conflicts of interest regarding this article.

References

Abbott, G.W. (2012). KCNE2 and the K^+ channel. Channels 6: 1–10.

Alkire, M.T., Asher, C.D., Franciscus, A.M., and Hahn, E.L. (2009). Thalamic microinfusion of antibody to a voltage-gated potassium channel restores consciousness during anesthesia. Anesthesiology 110: 766–773.

Budde, T., Mager, R., and Pape, H.-C. (1992). Different types of potassium outward current in relay neurons acutely isolated from the rat lateral geniculate nucleus. Eur. J. Neurosci. 4: 708–722.

Cazzin, C., Piccoli, L., Massagrande, M., Garbati, N., Michielin, F., Knaus, H.G., Ring, C.J.A., Morrison, A.D., Merlo-Pich, E., Rovo, Z., et al. (2011). rKv1.2 overexpression in the central medial thalamic area decreases caffeine-induced arousal. Gene Brain Behav. 10: 817–827.

Decher, N., Bundis, F., Vajna, R., and Steinmeyer, K. (2003). KCNE2 modulates current amplitudes and activation kinetics of HCN4: influence of KCNE family members on HCN4 currents. Pflügers Archiv 446: 633–640.

Decher, N., Streit, A.K., Rapedius, M., Netter, M.F., Marzian, S., Ehling, P., Renigunta, V., Ko, A., Dodel, R.C., Navarro-polanco, R.a, et al. (2010). RNA editing modulates the binding of drugs and highly unsaturated fatty acids to the open pore of Kv potassium channels. EMBO J. 29: 2101–2113.

Dodson, P.D. and Forsythe, I.D. (2004). Presynaptic K+ channels: electrifying regulators of synaptic terminal excitability. Trends Neurosci. 27: 210–217.

Han, Y., Lyman, K.A., Foote, K.M., and Chetkovich, D.M. (2020). The structure and function of TRIP8b, an auxiliary subunit of hyperpolarization-activated cyclic-nucleotide gated channels. Channels 14: 110–122.

He, C., Chen, F., Li, B., and Hu, Z. (2014). Neurophysiology of HCN channels: from cellular functions to multiple regulations. Prog. Neurobiol. 112: 1–23.

Heuermann, R.J., Jaramillo, T.C., Ying, S.-W., Suter, B.A., Lyman, K.A., Han, Y., Lewis, A.S., Hampton, T.G., Shepherd, G.M.G., Goldstein, P.A., et al. (2016). Reduction of thalamic and cortical Ih by deletion of TRIP8b produces a mouse model of human absence epilepsy. Neurobiol. Dis. 85: 81–92.

Hopkins, W.F. (1998). Toxin and subunit specificity of blocking affinity of three peptide toxins for heteromultimeric, voltage-gated potassium channels expressed in Xenopus oocytes. J. Pharmcol. Exp. Ther. 285: 1051–1060.

Huang, Z., Walker, M.C., and Shah, M.M. (2009). Loss of dendritic HCN1 subunits enhances cortical excitability and epileptogenesis. J. Neurosci. 29: 10979–10988.

Kanyshkova, T., Broicher, T., Meuth, S.G., Pape, H.-C., and Budde, T. (2011). A-type K^+ currents in intralaminar thalamocortical relay neurons. Pflügers Archiv 461: 545–556.

Kanyshkova, T., Meuth, P., Bista, P., Liu, Z., Ehling, P., Caputi, L., Doengi, M., Chetkovich, D.M., Pape, H.C., and Budde, T. (2012). Differential regulation of HCN channel isoform expression in thalamic neurons of epileptic and non-epileptic rat strains. Neurobiol. Dis. 45: 450–461.

Kasten, M.R., Rudy, B., and Anderson, M.P. (2007). Differential regulation of action potential firing in adult murine thalamocortical neurons by Kv3.2, Kv1, and SK potassium and N-type calcium channels. J. Physiol. 584: 565–582.

Krichmar, J.L., Nasuto, S.J., Scorcioni, R., Washington, S.D., and Ascoli, G.A. (2002). Effects of dendritic morphology on CA3 pyramidal cell electrophysiology: a simulation study. Brain Res. 941: 11–28.

Lewis, A.S., Schwartz, E., Chan, C.S., Noam, Y., Shin, M., Wadman, W.J., Surmeier, D.J., Baram, T.Z., Macdonald, R.L., and Chetkovich, D.M. (2009). Alternatively spliced isoforms of TRIP8b differentially control h channel trafficking and function. J. Neurosci. 29: 6250–6265.

Lewis, A.S., Vaidya, S.P., Blaiss, C.A., Liu, Z., Stoub, T.R., Brager, D.H., Chen, X., Bender, R.A., Estep, C.M., Popov, A.B., et al. (2011). Deletion of the hyperpolarization-activated cyclic nucleotide-gated channel auxiliary subunit TRIP8b impairs hippocampal Ih localization and function and promotes antidepressant behavior in mice. J. Neurosci. 31: 7424–7440.

Ludwig, A., Budde, T., Stieber, J., Moosmang, S., Wahl, C., Holthoff, K., Langebartels, A., Wotjak, C., Munsch, T., Zong, X., et al. (2003). Absence epilepsy and sinus dysrhythmia in mice lacking the pacemaker channel HCN2. EMBO J. 22: 216–224.

Oniani, T., Vinnenberg, L., Chaudhary, R., Schreiber, J.A., Riske, K., Williams, B., Pape, H.-C., White, J.A., Junker, A., Seebohm, G., et al. (2022). Effects of axonal demyelination, inflammatory cytokines and divalent cation chelators on thalamic HCN channels and oscillatory bursting. Int. J. Mol. Sci. 23: 6285.

Rhodes, K.J., Keilbaugh, S.A., Barrezueta, N.X., Lopez, K.L., and Trimmer, J.S. (1995). Association and colocalization of K^+ channel alpha- and beta-subunit polypeptides in rat brain. J. Neurosci. 15: 5360.

Robbins, C.A. and Tempel, B.L. (2012). Kv1.1 and Kv1.2: similar channels, different seizure models. Epilepsia 53: 134–141.

Rodrigues, A.R.A., Arantes, E.C., Monje, F., Stühmer, W., and Varanda, W.A. (2003). Tityustoxin-K(alpha) blockade of the voltage-gated potassium channel Kv1.3. Br. J. Pharmacol. 139: 1180–1186.

Sánchez-Ponce, D., DeFelipe, J., Garrido, J.J., and Muñoz, A. (2012). Developmental expression of Kv potassium channels at the axon initial segment of cultured hippocampal neurons. PLoS One 7: e48557.

Santoro, B., Hu, L., Liu, H., Saponaro, A., Pian, P., Piskorowski, R.a, Moroni, A., and Siegelbaum, S.a. (2011). TRIP8b regulates HCN1 channel trafficking and gating through two distinct C-terminal interaction sites. J. Neurosci. 31: 4074–4086.

Santoro, B., Piskorowski, R.A., Pian, P., Hu, L., Liu, H., and Siegelbaum, S.A. (2009). TRIP8b splice variants form a family of auxiliary subunits that regulate gating and trafficking of HCN channels in the brain. Neuron 62: 802–813.

Santoro, B., Wainger, B.J., and Siegelbaum, S.a. (2004). Regulation of HCN channel surface expression by a novel C-terminal protein-protein interaction. J. Neurosci. 24: 10750–10762.

Strutz-Seebohm, N., Gutcher, I., Decher, N., Steinmeyer, K., Lang, F., and Seebohm, G. (2007). Comparison of potent Kv1.5 potassium channel inhibitors reveals the molecular basis for blocking kinetics and binding mode. Int. J. Exp. Cell. Physiol. Biochem. Pharmacol. 20: 791–800.

Vennekamp, J., Wulff, H., Beeton, C., Calabresi, P.A., Grissmer, S., Hänsel, W., and Chandy, K.G. (2004). Kv1.3-Blocking 5-phenylalkoxypsoralens: a new class of immunomodulators. Mol. Pharmacol. 65: 1364–1374.

Werkman, T.R., Gustafson, T.A., Rogowski, R.S., Blaustein, M.P., and Rogawski, M.A. (1993). Tityustoxin-K alpha, a structurally novel and highly potent K^+ channel peptide toxin, interacts with the alpha-dendrotoxin binding site on the cloned Kv1.2 K^+ channel. Mol. Pharmacol. 44: 430–436.

Willis, M., Leitner, I., Seppi, K., Trieb, M., Wietzorrek, G., Marksteiner, J., and Knaus, H.G. (2018). Shaker-related voltage-gated potassium channels Kv1 in human hippocampus. Brain Struct. Funct. 223: 2663–2671.

Xiao, Y., Yang, J., Ji, W., He, Q., Mao, L., and Shu, Y. (2021). A- and D-type potassium currents regulate axonal action potential repolarization in midbrain dopamine neurons. Neuropharmacology 185: 108399.

Yee, J.X., Rastani, A., and Soden, M.E. (2022). The potassium channel auxiliary subunit Kvβ2 (Kcnab2) regulates Kv1 channels and dopamine neuron firing. J. Neurophysiol. 128: 62–72.

Ying, S.W., Kanda, V.A., Hu, Z., Purtell, K., King, E.C., Abbott, G.W., and Goldstein, P.A. (2012). Targeted deletion of Kcne2 impairs HCN channel function in mouse thalamocortical circuits. PLoS One 7: e42756.

Zemel, B.M., Ritter, D.M., Covarrubias, M., and Muqeem, T. (2018). A-type KV channels in dorsal root ganglion neurons: diversity, function, and dysfunction. Front. Mol. Neurosci. 11: 1–17.

Zobeiri, M., Chaudhary, R., Blaich, A., Rottmann, M., Herrmann, S., Meuth, P., Bista, P., Kanyshkova, T., Lüttjohann, A., Narayanan, V., et al. (2019). The hyperpolarization-activated HCN4 channel is important for proper maintenance of oscillatory activity in the thalamocortical system. Cerebr. Cortex 29: 2291–2304.

Zobeiri, M., Chaudhary, R., Datunashvili, M., Heuermann, R.J., Lüttjohann, A., Narayanan, V., Balfanz, S., Meuth, P., Chetkovich, D.M., Pape, H.-C., et al. (2018). Modulation of thalamocortical oscillations by TRIP8b, an auxiliary subunit for HCN channels. Brain Struct. Funct. 223: 1537–1564.

Supplementary Material: This article contains supplementary material (https://doi.org/10.1515/hsz-2023-0116).